THE EFFECTS OF NUCLEAR FORCES ON THE MAXIMUM MASS LIMIT OF NEUTRON STARS*

by

SACHIKO TSURUTA**
Goddard Space Flight Center
Greenbelt, Maryland

Recently the problem of the maximum mass limit of a stable neutron star has drawn the attention of many people, because it may seriously affect the models of pulsars and other phenomena which are most likely caused by the presence of neutron stars. In this brief report I wish to compare the neutron star models by various groups, including the most recent results I am aware of, those by the Cornell group (Boozer-Salpeter) and those by the Kyoto group (S. Ikeuchi, T. Mizutani, S. Nagata, R. Tamagaki, and C. Hayashi).

In Figure 1, the curve marked IDEAL represents the models with no nuclear interactions, originally constructed by Oppenheimer and Volkoff.[1] The models by Harrison, Thorne, Wakano and Wheeler[2] approximately lie on the same curve in the neutron star region. The dotted curves marked V_β and V_γ are the models constructed by Tsuruta and Cameron[3] and subsequently used by Thorne and others at CIT[4] in their calculations of the moments of inertia of neutron stars, etc. I decided to show these curves also, because these results (especially the V_γ models) have been used by Ostriker and others[5] in their pulsar studies. The solid curves show neutron star models

* Paper presented at the IAU Symposium No. 46 "The Crab Nebula," Nuffield Radio Astronomy Laboratories, Jodrell Bank, England, August 5-7, 1970.

** NAS-NRC Research Associate presently at Goddard Space Flight Center.

constructed after the pulsar discovery. The curve (1) is by Cohen et al.[6], (2) is by the Cornell group (Boozer-Salpeter), (3) is by Wang et al.[7], and the curves (4) through (7) are obtained by the Kyoto group.

In all models shown here except the first (those marked IDEAL), nuclear interactions are taken into account. In the models marked as V_β and V_γ, the nuclear potentials of V_β and V_γ type, respectively, by Levinger and Simmons[8] are used. In the models (1), the modified Levinger-Simmons neutron gas models are used. Boozer and Salpeter (the curve (2)) made use of the neutron gas calculations (2b) by Nemeth and Sprung[9] with the soft-core Reid potentials. Wang et al. (the curve (3)) took the average of the soft-core Reid potentials and several other potentials, but they all give the similar equations of state. The results by the Kyoto group are obtained in the following way. For densities ρ less than $\rho_o \simeq 8 \times 10^{14}$ gm/cm^3 where the neutron matter calculations from the concept of "nuclear potential" becomes unreliable, the one-boson exchange hard-core potentials constructed by Kishi were used in the models (4), called OBEP-K, and the one-pion exchange potentials with a Gaussian type soft core constructed by Tamagaki were used in the models (5) called OPEG-T. For $\rho > \rho_o$ in these models, the equation of state obtained in this manner was parabolically extrapolated in the logarithmic scale. In the models (6) and (7), the equation of state $P = \epsilon/3$ and $P = \epsilon$, respectively, (where ϵ is the energy density) were used for $\rho > \rho_1 \simeq 5 \times 10^{15}$ gm/cm^3 where the Zel'dovich type scalar or vector interactions are assumed to become applicable, the method (4) was used for $\rho \lesssim \rho_o$, and the intermediate regions have been interpolated. Similar results are obtained if the OPEG-T or the Hamada-Johnston potentials are used for $\rho \lesssim \rho_o$.

We see, first of all, that drastically different masses are obtained depending on how the inter-particle interaction problem is treated. In the models (2) and (3) the calculations are terminated where the nuclear potential approach is thought to become unreliable. If the calculations are extended to higher densities, the curve (2) reaches the mass peak of about 1 $M_\odot$, similar to the curves (4) and (5) by the Kyoto group. Near the breakdown point, ρ_o, the models (3), (4), (5), (6) and V_β have small mass values of only around 0.2-0.4 $M_\odot$, while the other models shown in the figure have larger masses. At the mass peak, the curve (7) reaches almost 3$M_\odot$. It may be pointed out that these models obtained by different methods nevertheless possess a few common points as mentioned below. As the mass increases from the minimum value to approximately 0.2$M_\odot$, the corresponding radius decreases quickly from about 300 km to about 10 km or so. This occurs a little below or around the nuclear density, depending on the models. For densities of around 10^{15} gm/cm^3 the radius is around 10 km, and for densities of around 10^{16} gm/cm^3 the radius is around 5 km. Our studies also show that the effects of the presence of hyperons and protons on the mass limit are much smaller than the effects of nuclear forces, if the interactions among all baryons are basically similar. It will be hard to draw definite conclusions from the above results, but the following comments may be valid.

In the regions where the concept of "nuclear potential" is still valid (for approximately $\rho \lesssim 10^{15}$ gm/cm^3), using realistic potentials alone is not enough. For instance, quite different results are obtained in the models (2) and (3), even though the both groups used the similar potentials (the soft-core Reid potentials). In this respect (of applying realistic potentials in a realistic way), I feel that the models (5), the OPEG-T, are the best recommended (among the models shown here). However, it may

be noted that many-body interactions are generally neglected and that the nuclear potential term is treated non-relativistically in the work done so far. The net effect of the corrections to these approximations seems to lower the densities and increase the masses near the mass peak. Thus the V_γ models used already in various pulsar studies seem to be not far from reality.

The exact behavior in the regions above about 10^{15} gm/cm^3 seems to be beyond the knowledge of present-day physics. Since the maximum mass of some of the models lie in these high density regions, it is hard to answer the question of how high masses stable neutron stars can have. It will be fortunate if such a question can be answered rather from the observational side. Will it be an impossible dream, if one contemplates that more detailed pulsar observations might help the break-through of the difficulties facing us today in particle physics and some other fields?

In the pre-pulsar discovery periods, I did not see much sense in going beyond our V_β and V_γ models of neutron stars. But, today, with more observations of pulsars becoming available, better theoretical work with the cooperation of experts in various fields, including the effort to construct more realistic neutron star models, seems very desirable.

I wish to thank Professors Hayashi, Nagata, Salpeter and Tamagaki, and Messrs. Boozer, Ikeuchi and Mizutani, for giving me the results of their calculations[10] before publications.

Outputs Generated through AI:

Title:

“NEUTRON STAR MODELS”

Summary:

The report was produced by the nasa center for aerospace information casi. It shows the effects of nuclear forces on the maximum mass limit of neutron stars. It also shows the neutron star models by various groups including the most recent results.

Important Keywords:

'Models', 'neutrons', 'used', 'nuclear', 'mass', 'potentials','results', 'curve', 'obtained'.

Keywords Visualization:

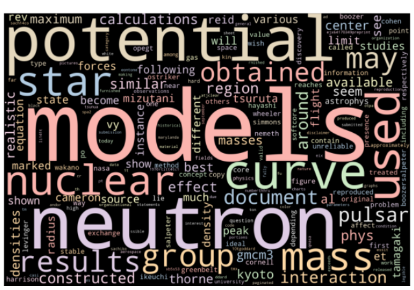

Word Cloud

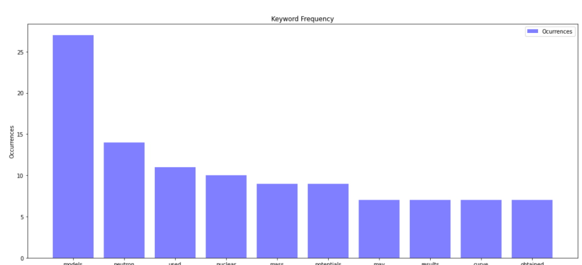

Keywords Count

NTRS Document Preview

THE PREDICTION OF CORONAL AND INTERPLANETARY MAGNETIC FIELDS

K. H. Schatten
Laboratory for Extraterrestrial Physics
NASA-Goddard Space Flight Center
Greenbelt, Maryland 20771

Abstract

The advent of high speed digital computers and advances in the understanding of the solar atmosphere have enabled predictions of solar eclipse structure. The magnetic field models, their applications, and limitations are discussed. The effects of solar activity on coronal structure are also discussed. Severny, Wilcox, Scherrer, and Colburn have recently shown that a high degree of correlation exists between the mean photospheric field and the interplanetary magnetic field. A means for predicting the interplanetary magnetic field is a consequence of their work. An interpretation of this effect is presented that relates to models of the coronal magnetic field.

I. Introduction

Predictions of solar eclipse occurrences provide us with tests of classical mechanics and information concerning the sun, moon and earth. In a similar manner, recent predictions and observations of solar eclipse structure provide tests of our understanding of astrophysical plasmas and yield new data concerning the behavior of the solar corona.

Early evidence of the importance of the magnetic field in coronal structuring processes was obtained by analogy between the shape of the beautiful polar plumes of the solar corona and the patterns formed by iron filings placed near a bar magnet. Later evidence came with observations of solar magnetism and more recently with the discovery of the solar wind (e.g., Hale;(1) Hale and Nicholson;(2) Chapman and Ferraro;(3) Biermann;(4) Chapman;(5) Parker;(6) and Weber and Davis(7)). The presence of a magnetic field embedded within the solar wind that is directly related to the solar magnetic field has been shown by Ness and Wilcox.(8)

This leads up to the present day treatment of the interaction of the coronal and interplanetary magnetic field and plasma.

II. Coronal Magnetic Models

An understanding of the magnetic models of Schatten, Wilcox and Ness(9) and Altschuler and Newkirk(10) may be aided by referring to Figure 1. This shows the energy density of various components of the solar atmosphere as a function of distance above the photosphere. The data for the figure were obtained by choosing moderate values for the densities, velocities, temperatures and magnetic field strengths within the solar cycle. The energy curves shown are to be interpreted from a somewhat qualitative viewpoint in that uncertainties are likely to be near a factor of 10, and the representation of complex coronal structures by average values is somewhat misleading. Nevertheless, the curves do show the

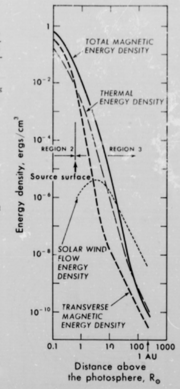

Figure 1. The coronal energy density of the total magnetic field, transverse magnetic field, thermal motion, and solar wind flow versus distance above the photosphere. In region 2 the magnetic field dominates the structure. On the source surface currents flow which allow the field to be transported by the solar wind.

relative importance of various components of the solar corona. Close to the sun, both the magnetic field and the transverse magnetic field predominate, indicating that a force free field configuration results. Beyond about 0.6 solar radii, the coronal plasma thermal energy density supersedes the transverse field energy density. This allows the plasma to stream away from the sun and the field becomes predominantly radial. The Alfvén point is near 20 or 30 solar radii. This is the region where the flow energy density exceeds the field energy density and thus the flow is super-Alfvénic. Escape of the plasma is inevitable beyond this point. Weber and Davis(7) give an excellent description of this region.

The topology of the magnetic field in the solar corona as suggested by the magnetic models may be examined in Figure 2. There are three distinct regions in these models where different physical phenomena occur. Region 1 represents the photosphere, where the magnetic field motion is governed by the detailed motions of the plasma near the photosphere. Above the photosphere the plasma density diminishes very rapidly with only moderate decreases in the magnetic energy density. This results in region 2, where the magnetic energy density is greater than the plasma energy density and hence controls the configuration. One may then utilize the force-free condition, $\mathbf{j} \times \mathbf{B} = 0$, and in fact make the more restrictive assumption that region 2 is current free. The magnetic field in region 2 may then be derived from a potential that obeys the Laplace equation: $\nabla^2 \phi = 0$. The scalar potential may then be employed in this region.

Substantially further out in the corona the total magnetic energy density diminishes to a value less than the plasma energy density, and the magnetic field can no longer structure the solar wind flow. The magnetic field has, however, become oriented very much in the radial direction, as suggested by Davis.(11) Thus, before the total magnetic energy density falls below the plasma energy density, a region is reached where the transverse magnetic energy density does so. It is the transverse magnetic field that interacts with the coronal plasma, since a radial magnetic field would neither affect nor be affected by a radially flowing plasma. Regions 2 and 3 are separated by the surface where the transverse magnetic energy density falls below the plasma energy density. In region 3 transverse magnetic fields are transported by the radially flowing plasma, and can not exist in a quasi-static fashion. The magnetic field existing on the surface boundary between regions 2 and 3 is thus oriented in approximately the radial direction, and serves as a source for the interplanetary magnetic field.

Figure 3 shows this "source surface" superposed upon drawings of coronal eclipse structure from the February 15, 1961 eclipse (by Vsekhsvjatsky,(12) top) and the February 25, 1952 eclipse (by Nikolskij,(13) bottom). The closed arches fall within the "source surface" sphere. Beyond this distance structures are oriented more nearly radial, in accordance with the model.

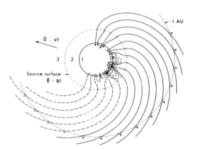

Figure 2. Schematic representation of the source surface model. The photospheric magnetic field is measured in region 1 at Mount Wilson Observatory. Closed field lines (loops) exist in region 2. The field in this region is calculated from potential theory. Currents flowing near the source surface eliminate the transverse components of the magnetic field, and the solar wind extends the source surface magnetic field into interplanetary space. The magnetic field is then observed by spacecraft near 1 AU.

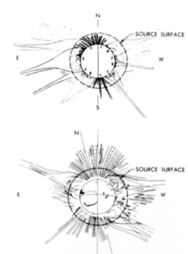

Figure 3. Drawing of the February 15, 1961 eclipse (Vsekhsvjatsky, 1963) (top). Drawing of the corona during the February 25, 1952 eclipse (Nikolskij, 1953) (bottom).

Both the Altschuler and Newkirk and the Schatten, Wilcox and Ness magnetic models are based upon similar physical mechanisms. Only the mathematics in handling the solution and in approximating the observed photospheric magnetic fields differ. Altschuler and Newkirk(10) have claimed their technique is superior in its mathematical sophistication. Schatten(14) agrees with their mathematical improvements in theory. In practice, however, Schatten(14) suggests that uncertainties in the measured photospheric vector magnetic field and in accounting properly for the effects of the coronal plasma outweigh the differences in the two computational techniques.

III. Comparison of Solutions With Eclipse Observations

Comparisons of magnetic field calculations with solar eclipse observations were made for the November 12, 1966 eclipse utilizing both techniques. Figure 4 shows the results of Altschuler and Newkirk(10) and Figure 5 that of Schatten.(15) Both calculations agree moderately well with each other and with the structure observed in the solar eclipse. It is important to note that there was not very much solar activity prior to this solar eclipse.

The comparisons of computed magnetic fields with observed coronal structure provided encouraging tests of the validity of the models. Other tests were performed as well. The extended coronal magnetic field compared well with the observed interplanetary magnetic field (Schatten, Wilcox and Ness(9)). In addition, a Faraday rotation experiment provided information on the coronal magnetic field from 4-12 solar radii that agreed with calculations based on the model of Schatten, Wilcox and Ness (see Stelzried et al.(16)).

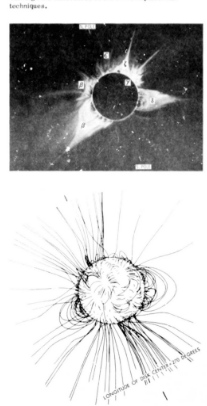

Figure 4. A sketch of the solar corona of November 12, 1966 used to display time scale features (top). Magnetic field line map (bottom) for November 12, 1966 (after Altschuler and Newkirk).

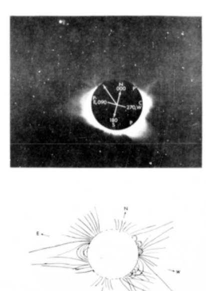

Figure 5. Photograph of the solar corona of November 12, 1966 (top). Sketch of magnetic field line structure for the November 12, 1966 solar eclipse by Schatten (bottom). Note similarity with Figure 4.

Outputs Generated through AI:

Title:

PREDICTION CORONAL INTERPLANETARY

Summary:

This document is the best reproduction from the original submission. It was produced by the nasa center for aerospace information casi in 1970. It is about the prediction of coronal and interplanetary magnetic fields and the effects of solar activity on coronal structures. It also covers the predictions of solar eclipse occurrences.

Important Keywords:

'Field','solar','magnetic','coronal','eclipse','structure', 'region, 'corona', 'source','plasma.

Keywords Visualization:

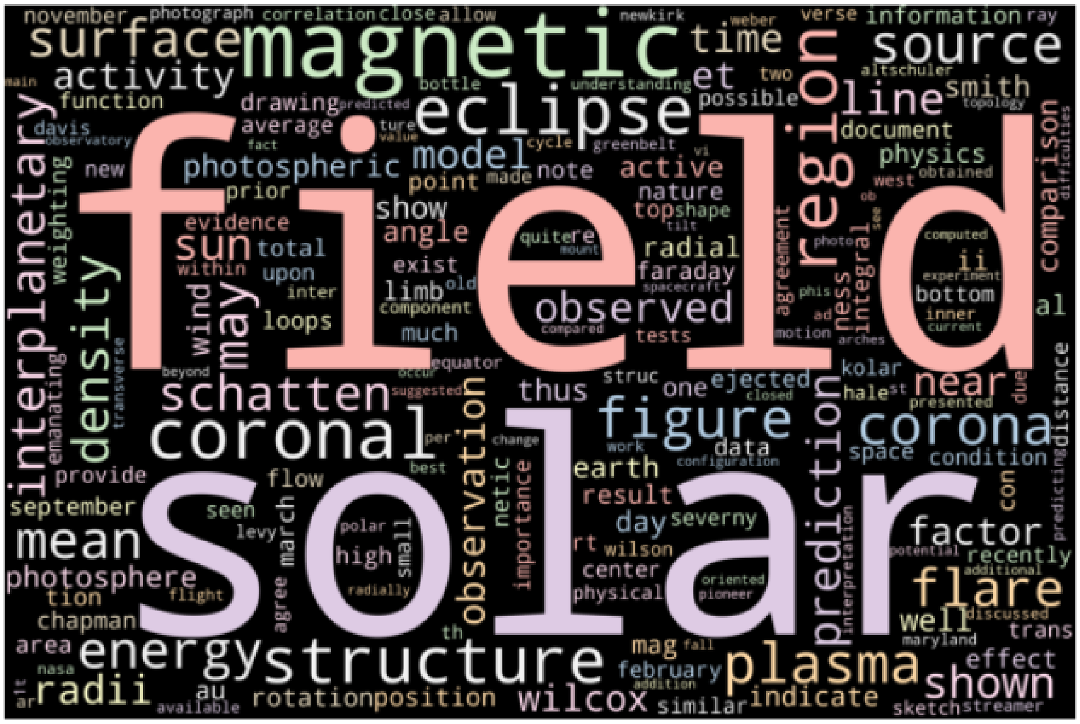

Word Cloud

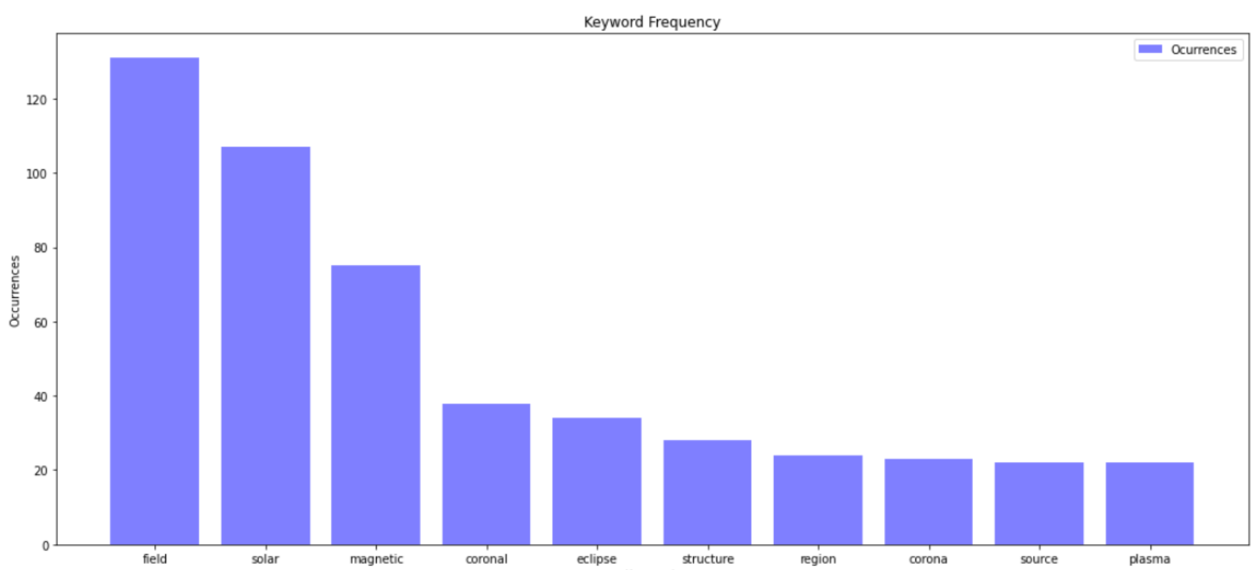

Keywords Count

N90-26781

STUDY OF POLYOXYMETHYLENE AND ITS SPUTTERED FRAGMENTS-- IMPLICATIONS FOR COMETS

Marla H. Moore* and Toshihiko Tanabe**

*University of Maryland, Dept. of Chem., College Park, MD 20742
**NRC-NASA/GSFC, Code 691, Greenbelt, MD 20771

ABSTRACT

Laboratory mass spectra of sputtered polyoxymethylene, POM, reveals a fragmentation pattern consistent with observed peaks in the PICCA experiment on board the Giotto spacecraft. Both commercially available POM and radiation synthesized POM have been used in our studies. Synthesized POM was identified using infrared absorption spectra after proton irradiation of H_2CO ice on silicate grains at 20K. Laboratory results suggest that similar type sputtering is a possible mechanism for removing species from comet grains.

INTRODUCTION

A complex line of evidence for a form of formaldehyde (H_2CO) in comet Halley came from the interpretation of data from the PICCA instrument on board Giotto. In the inner coma a repeating mass spectral pattern with peak centers at the approximate locations of 45, 61, 75, 91, 105, and 121 amu was detected. Mitchell et al.[1], Huebner and Boice[2], and Huebner[3] suggested the mass spectrum could be fit with the fragmentation pattern of the polymerized form of H_2CO known generically as polyoxymethylene, POM.

The idea that POM could be present in cometary materials is not new. Wickramasinghe[4,5] proposed that H_2CO condenses on interstellar silicate grains as polyoxymethylene and the possibility of this polymer in cometary dust was discussed by Vanysek and Wickramasinghe[6]. Laboratory experiments by Goldanskii et al.[7] showed that irradiation of condensed H_2CO synthesized polyoxymethylene to temperatures below 20K and Goldanskii[8] discussed the possibility of similar radiation synthesis in ices in molecular clouds. In our laboratory experiment radiation synthesized POM was identified by its infrared absorption features.

EXPERIMENTAL RESULTS

We have sputtered POM in vacuum at 300K using 700KeV protons and recorded the mass spectrum. Fragments are observed at 45, 61, 75, 91, 105 121 and 135 amu and these results are compared with the PICCA data in Figure 1. As shown in Table I, these peaks can be assigned to the fragmentation products of POM with an alternating CH_3 or H end group. The 700KeV proton beam current was near

TABLE I: TENTATIVE ASSIGNMENT OF POM FRAGMENTATION PEAKS

m/e	ION+	m/e	ION+
45	$(H_2CO)CH_3$		
61	$(H_2CO)_2H$	60	$(H_2CO)_2$
75	$(H_2CO)_2CH_3$		
91	$(H_2CO)_3H$	89	$(H_2CO)_2HCO$
105	$(H_2CO)_3CH_3$		
121	$(H_2CO)_4H$	119	$(H_2CO)_3HCO$
135	$(H_2CO)_4CH_3$	131&133	unidentified

1.5×10^{-7} amps (corresponding to 2×10^{11} protons/cm^2-sec). In the region of mass 30 the quadrupole mass spectrometer was saturated and the resulting overlaid data in Figure 1 spanned more than 3 log pressure scales in intensity. All data points had the background subtracted automatically and were recorded using the electron multiplier. A 70 eV electron ionizer voltage was used for these experiments.

Sputtering of thin films of commercially available paraformaldehyde (a polyoxymethylene glycol) gave the same results as sputtered POM synthesized in our laboratory. Other peaks recorded in our sputtered spectrum are listed in Table I and two can be attributed to fragments of POM with an attached HCO group.

In contrast, using direct insertion techniques the mass spectrum of solid polyoxymethylene glycol was analyzed by Moller

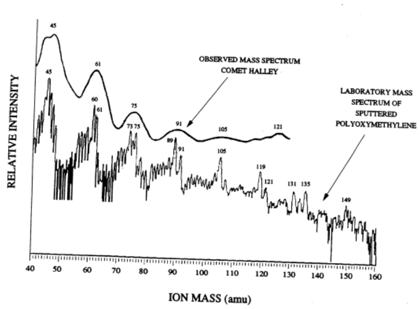

FIGURE 1. The upper curve reproduces the mass spectrum measured by the PICCA instrument on board the GIOTTO spacecraft in the inner coma of comet Halley. This is compared with our laboratory mass spectrum of fragments produced during sputtering polyoxymethylene at 300 K with 700 KeV protons.

and Jackson[9]. At 300K peaks were observed at 47, 61, 77, 91, 107, 121 amu, consistent with a fragmenting polymer with alternating H and OH groups attached. The peaks do not fit the central peak assignments of the PICCA spectrum but could contribute to its width.

Figure 2A shows the infrared spectrum from 2.5um to 25um of an amorphous silicate smoke. It's dominate SiO stretch feature is near 10um, the SiO bend is near 21um. H_2CO gas was condensed onto this smoke at 20K and the resulting ice-silicate was irradiated with 700KeV protons to a total incident dose of 1.5×10^{15} protons/cm^2. Polymerization of formaldehyde occurred at 20K and the POM remained on the silicate when warmed to 300K. The infrared spectrum of the POM-silicate is shown in Figure 2B. The ratio spectrum (POM-silicate/silicate) in Figure 2C reveals the major absorptions of POM on silicate at 8.99um and 10.7um. This sample was subsequently sputtered.

CONCLUSION

Our laboratory results suggest that sputtering of POM is a possible origin of the peaks measured in the PICCA data. Sputtering experiments in which solar wind type ions are used need to be studied since 700KeV protons are not dominate in the inner coma. Each PICCA peak appears to be composed of 3 or more closely spaced masses[1]. Sputtering of POM may contribute to the peak, but other processes such as sublimation may contribute to the width. Also we suggest that other complex non-volatile organic residues may exist on comets and fragments from these may be sputtered from grains in the coma contributing to the observed data. The study of sputtered fragments from other organic residues is currently under investigation.

Outputs Generated through AI:

Title:

CONCERNED SPACE NAVIGATION

Summary:

There is a technical note on the sale by the clearinghouse for federal scientific and technical information springfield virginia. It is a study aimed at simplifying the equations used when applying the kalman filter to space navigation. The transition matrix has been obtained by integrating the perturbation equations of motion.

Important Keywords:

'matrix','transition','matrices','time','navigation', 'used', 'equations','equation', 'trajectory', 'results'

Keywords Visualization:

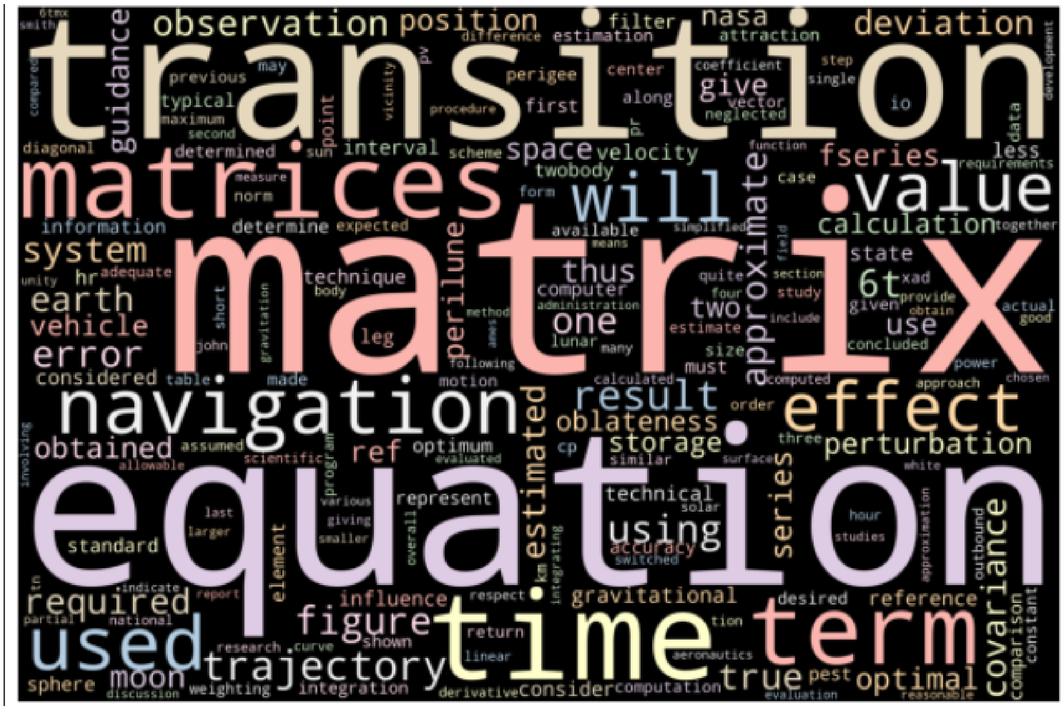

Word Cloud

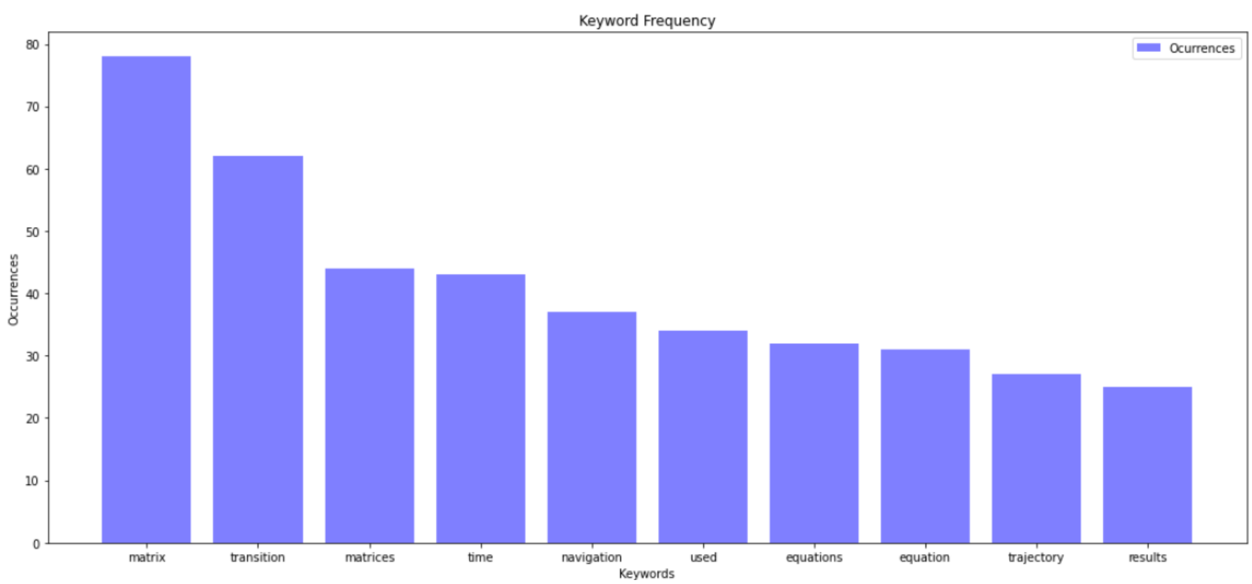

Keywords Count